Microfluidic tunable inkjet-printed metamaterial absorber on paper

Kenyu Ling,[1] Minyeong Yoo,[1] Wenjing Su,[2] Kyeongseob Kim,[1] Benjamin Cook,[2] Manos M. Tentzeris,[2] and Sungjoon Lim[1*]

[1]*School of Electrical and Electronic Engineering, Chung-Ang University, Heukseok-Dong, Dongjak-Gu 156-756, South Korea*

[2]*School of Electrical and Computer Engineering, Georgia Institute of Technology, Atlanta, Georgia 30519, USA*

[*]*sungjoon@cau.ac.kr*

Abstract: In this paper, we propose a novel microfluidic tunable metamaterial (MM) absorber printed on a paper substrate in silver nanoparticle ink. The metamaterial is designed using a periodic array consisting of square patches. The conductive patterns are inkjet-printed on paper using silver nanoparticle inks. The microfluidic channels are laser-etched on polymethyl methacrylate (PMMA). The conductive patterns on paper and the microfluidic channels on PMMA are bonded by an SU-8 layer that is also inkjet-printed on the conductive patterns. The proposed MM absorber provides frequency-tuning capability for different fluids in the microfluidic channels. We performed full-wave simulations and measurements that confirmed that the resonant frequency decreased from 4.42 GHz to 3.97 GHz after the injection of distilled water into the microfluidic channels. For both empty and water-filled channels, the absorptivity is higher than 90% at horizontal and vertical polarizations.

OCIS codes: (160.3918) Metamaterials; (260.5740) Resonance; (050.6624) Subwavelength structures.

References and links

1. D. R. Smith, J. B. Pendry, and M. C. Wiltshire, "Metamaterials and negative refractive index," Science **305**(5685), 788–792 (2004).
2. R. A. Shelby, D. R. Smith, and S. Schultz, "Experimental verification of a negative index of refraction," Science **292**(5514), 77–79 (2001).
3. D. Schurig, J. J. Mock, B. J. Justice, S. A. Cummer, J. B. Pendry, A. F. Starr, and D. R. Smith, "Metamaterial electromagnetic cloak at microwave frequencies," Science **314**(5801), 977–980 (2006).
4. B. Wang, T. Koschny, and C. M. Soukoulis, "Wide-angle and polarization-independent chiral metamaterial absorber," Phys. Rev. B **80**(3), 033108 (2009).
5. N. I. Landy, S. Sajuyigbe, J. J. Mock, D. R. Smith, and W. J. Padilla, "Perfect metamaterial absorber," Phys. Rev. Lett. **100**(20), 207402 (2008).
6. G. Keiser, K. Fan, X. Zhang, and R. Averitt, "Towards Dynamic, Tunable, and Nonlinear Metamaterials via Near Field Interactions: A Review," J. Infrared, Millimeter, and Terahertz Waves **34**(11), 709–723 (2013).
7. Y. Kotsuka, K. Murano, M. Amano, and S. Sugiyama, "Novel right-handed metamaterial based on the concept of "autonomous control system of living cells" and its absorber applications," IEEE Trans. Electromagn. Compat. **52**(3), 556–565 (2010).
8. C. Mias and J. H. Yap, "A varactor-tunable high impedance surface with a resistive-lumped-element biasing grid," IEEE Trans. Antenn. Propag. **55**(7), 1955–1962 (2007).
9. D. Shrekenhamer, W. C. Chen, and W. J. Padilla, "Liquid crystal tunable metamaterial absorber," Phys. Rev. Lett. **110**(17), 177403 (2013).
10. C. P. Ho, P. Pitchappa, Y. Lin, C. Huang, P. Kropelnicki, and C. Lee, "Electrothermally actuated microelectromechanical systems based omega-ring terahertz metamaterial with polarization dependent characteristics," Appl. Phys. Lett. **104**(16), 161104 (2014).
11. B. Wang, L. Wang, G. Wang, W. Huang, X. Li, and X. Zhai, "Frequency continuous tunable terahertz metamaterial absorber," J. Lightwave Technol. **32**(6), 1183–1189 (2014).
12. F. Alves, D. Grbovic, B. Kearney, and G. Karunasiri, "Microelectromechanical systems bimaterial terahertz sensor with integrated metamaterial absorber," Opt. Lett. **37**(11), 1886–1888 (2012).

#223429 - $15.00 USD Received 18 Sep 2014; revised 24 Nov 2014; accepted 10 Dec 2014; published 5 Jan 2015

13. T. S. Kasirga, Y. N. Ertas, and M. Bayindir, "Microfluidics for reconfigurable electromagnetic metamaterials," Appl. Phys. Lett. **95**(21), 214102 (2009).
14. L. Liu, A. R. Katko, D. Li, and S. A. Cummer, "Broadband electromagnetic metamaterials with reconfigurable fluid channels," Phys. Rev. B **89**(24), 245132 (2014).
15. A. Liu, W. Zhu, D. Tsai, and N. I. Zheludev, "Micromachined tunable metamaterials: a review," J. Opt. **14**(11), 114009 (2012).
16. M. Datta and L. T. Romankiw, "Application of chemical and electrochemical micromachining in the electronics industry," J. Electrochem. Soc. **136**(6), 285C–292C (1989).
17. B. S. Cook and A. Shamim, "Inkjet printing of novel wideband and high gain antennas on low-cost paper substrate," IEEE Trans. Antenn. Propag. **60**(9), 4148–4156 (2012).
18. H. Tao, L. R. Chieffo, M. A. Brenckle, S. M. Siebert, M. Liu, A. C. Strikwerda, K. Fan, D. L. Kaplan, X. Zhang, R. D. Averitt, and F. G. Omenetto, "Metamaterials on paper as a sensing platform," Adv. Mater. **23**(28), 3197–3201 (2011).
19. H. Tao, C. Bingham, A. Strikwerda, D. Pilon, D. Shrekenhamer, N. Landy, K. Fan, X. Zhang, W. Padilla, and R. Averitt, "Highly flexible wide angle of incidence terahertz metamaterial absorber: Design, fabrication, and characterization," Phys. Rev. B **78**(24), 241103 (2008).
20. W. Rechberger, A. Hohenau, A. Leitner, J. Krenn, B. Lamprecht, and F. Aussenegg, "Optical properties of two interacting gold nanoparticles," Opt. Commun. **220**(1), 137–141 (2003).
21. W. J. Padilla, A. J. Taylor, C. Highstrete, M. Lee, and R. D. Averitt, "Dynamical electric and magnetic metamaterial response at terahertz frequencies," Phys. Rev. Lett. **96**(10), 107401 (2006).
22. B. S. Cook, J. R. Cooper, and M. M. Tentzeris, "An inkjet-printed microfluidic RFID-enabled platform for wireless Lab-on-Chip applications," IEEE Trans. Microw. Theory Tech. **61**(12), 4714–4723 (2013).

1. Introduction

Electromagnetic (EM) metamaterials (MMs) are artificial structures whose properties are not observed in naturally occurring materials [1]. For example, negative permittivity and/or negative permeability can be realized by MMs [2]. MMs have been used to demonstrate electromagnetic cloaking [3] and to realize microwave/terahertz absorbers [4]. In 2008, an MM absorber was first proposed using the periodic structure of split-ring resonators (SRRs) and thin wires [5]. When the permittivity and permeability are manipulated, perfect absorptivity is achieved at the resonance frequency, even though it has a thin layer.

Nowadays, frequency-tunable MM absorbers have received attention for their wide spectrum operation, frequency-based sensors, and high-resolution image scanning applications [6]. Because of the electric/magnetic resonance of MM absorbers, frequency-tunable MM absorbers can be realized by using tunable devices such as PIN diodes [7], varactor diodes [8], liquid crystal [9], and microelectromechanical systems (MEMS) [10–12]. In this paper, we propose a frequency-tunable MM absorber using a novel tuning mechanism. Instead of conventional electronic tuning devices, microfluidic channels are loaded in order to change the resonant frequency for different fluidic materials inside capillary channels. It was reported that electromagnetic responses of MM can be controlled by fluid channels [13–15]. However, microfluidics have not been applied to frequency-tunable MM absorber applications.

In addition, all fabrications are processed without generating chemical waste. The conductive patterns are inkjet-printed on paper in silver nanoparticle inks, the microfluidic channels are laser-etched on polymethyl methacrylate (PMMA), and the bonding materials are inkjet-printed in SU-8 dielectric inks. Previously, most MM absorbers were realized using printed-circuit-board (PCB)-based chemical etching processes or micromachining processes in a clean room [16]. However, the proposed MM is realized using inkjet-printing technology, which is the first approach in MM absorber applications. The inkjet-printing process is an additive fabrication process that is eco-friendly because of its direct writing and because it generates no chemical waste. Compared to typical etching processes, the inkjet-printing process is much simpler and faster [17].

In this paper, we also propose a novel inkjet-printed MM absorber with frequency-tuning capability using microfluidic channels. The proposed absorber is the first microfluidically reconfigurable metamaterial absorber that uses inkjet-printing technology. Although the switching speed of microfluidics is slower than that of other electronic tunable devices, the

#223429 - $15.00 USD Received 18 Sep 2014; revised 24 Nov 2014; accepted 10 Dec 2014; published 5 Jan 2015

fluidic-controllable resonance of the proposed absorber is beneficial for wireless chemical or biosensor applications. Inkjet-printing technology and organic paper substrates provide additional advantages for low-cost sensor applications [18].

2. Absorber design

The MM absorber is designed with an EM resonator whose permittivity (ε) and permeability (μ) are tailored to match the impedance of the MM to the impedance of free space [19]. The impedance of the MM can be determined by the permittivity and permeability, as given by

$$Z_{MM}(\omega) \cong \sqrt{\mu(\omega)/\varepsilon(\omega)}. \quad (1)$$

If we calculate the proper effective permittivity and effective permeability, we will achieve perfect impedance match between the MM (Z_{MM}) and free space (Z_0 = 377 Ω), which means no reflection (Γ(ω)) at the surface of the MM from the following equation:

$$\Gamma(\omega) = \frac{Z_0 - Z_{MM}(\omega)}{Z_0 + Z_{MM}(\omega)}. \quad (2)$$

Figure 1 shows a simple square patch, which is introduced as the unit cell of the proposed MM absorber. Since the bottom layer is completely grounded by a metal film, the transmitted wave T(ω) is minimized, and the proposed absorber can achieve high absorptivity A(ω), as given by

$$A(\omega) = 1 - \Gamma(\omega) - \mathrm{T}(\omega). \quad (3)$$

The resonance is originated by a dipolar coupling between two adjacent unit cells [20]. Therefore, the dipole resonance of the proposed absorber is determined by the side length of the square patch (b) and the gap between two adjacent unit cells (s). As a result, the resonance frequency f_r is approximately calculated by

$$f_r \cong \frac{c}{2(2b+s)\sqrt{\varepsilon_{avg}}}. \quad (4)$$

where c is the velocity of light, and ε_{avg} is the average dielectric constant around the gap between two unit cells [21].

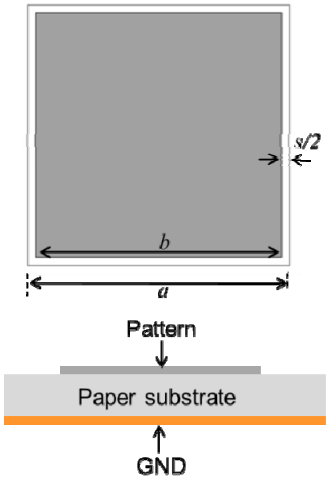

Fig. 1. Top and side view of the unit cell of the MM absorber: a = 16 mm, b = 15 mm, s = 1 mm.

#223429 - $15.00 USD Received 18 Sep 2014; revised 24 Nov 2014; accepted 10 Dec 2014; published 5 Jan 2015

From Eq. (4) we know that the resonance frequency of the MM is dependent on both the geometrical dimensions of the conductive pattern and the average dielectric constant. Since the geometrical dimensions are much less likely to change after fabrication, we can have full use of the change in dielectric constant to achieve tuning ability. Compared to the air, liquid such as water has a higher dielectric constant. When a liquid is loaded on the surface of the unit cell, the dielectric constant will change significantly. As a result, the resonance frequency will vary with the properties of the fluid on the surface. The proposed tuning mechanism is material dependent, while varactor diodes or MEMS are voltage dependent. Therefore, the microfluidic technology does not require a complex bias network design or DC power consumption.

To design the microfluidic channel, we first need to determine its location. In order to make the resonant frequency sensitive to fluids, the microfluidic channel is placed in a location where electric fields are strongly coupled. From Fig. 2(a), this is determined to be at the center of the gap, where the simulated electric field distribution of the unit cell is plotted before loading the microfluidic channel. In our study, we used a finite-element-method (FEM)-based ANSYS high-frequency structure simulator (HFSS) for full-wave analysis. From material characterization, the dielectric constant and loss tangent of the paper are determined to be 3.22 and 0.09, respectively.

From Fig. 2(b), we observe that antiparallel currents flow on the top and bottom conductive layers. This results in magnetic coupling with the incident magnetic field. Note that the electric current is weak at the gap. Therefore, the microfluidic channels are weakly coupled to the magnetic fields. In addition, it is expected that the microfluidic channels on the top patches will not affect the EM resonance of the MM, and only microfluidic channels on the gap will affect the electric response of the MM.

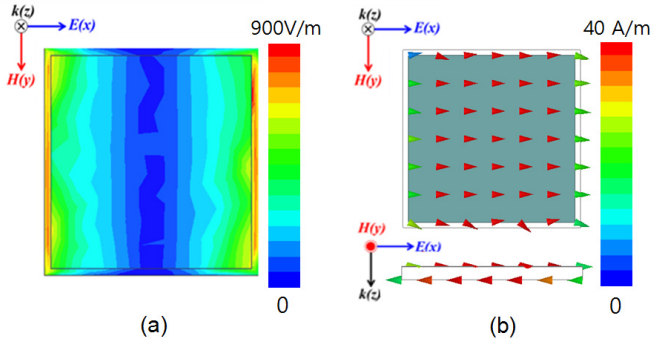

Fig. 2. Full-wave simulated distributions of (a) magnitude of electric field and (b) resonant electric current vector.

#223429 - $15.00 USD Received 18 Sep 2014; revised 24 Nov 2014; accepted 10 Dec 2014; published 5 Jan 2015

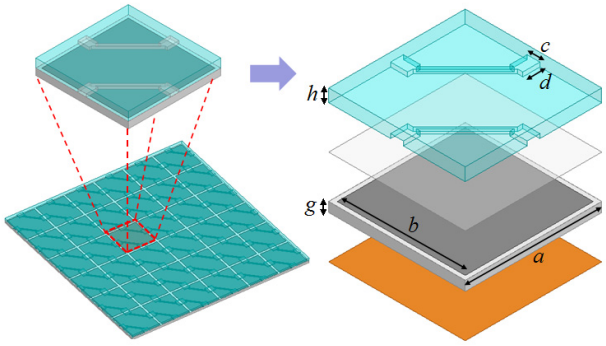

Fig. 3. Illustration of the proposed microfluidic MM absorber and its unit cell. Dimensions: c = 1.5 mm, d = 2 mm, g = 1.13 mm, and h = 1.5 mm.

Next, we determine the dimensions of the microfluidic channels. Figure 3 shows the unit cell of the proposed microfluidic MM absorber. The unit cell consists of the microfluidic layer, bonding layer, and MM absorber layer. The MM is designed with a square patch on paper. The microfluidic channel is designed on PMMA with a 1.5-mm thickness. The dielectric constant and loss tangent of the PMMA are 3.22 and 0.02, respectively. The width (c) and length (d) of the channel are determined in order to satisfy both highly sensitive frequency tunability and high absorptivity for various fluidic materials. A larger microfluidic channel results in a greater sensitivity to changes in frequency.

Figure 4(a) shows the reflection coefficients when the width (c) is 0.5 mm, 1.5 mm, and 2.5 mm when the length (d) is kept at 2 mm. The microfluidic channels are filled with distilled water because the reflection coefficients do not change when the channel is empty, although the channel dimensions are changed. As expected, the resonant frequency decreases with a wider channel (larger c). However, because the reflection coefficient increases, the absorption ratio also decreases. Therefore, we designed the microfluidic channel with c = 1.5 mm in order to satisfy the conditions for a reflection coefficient larger than −15 dB. Figure 4(b) shows the reflection coefficient when the length (d) is 1 mm, 1.5 mm, 2 mm, and 2.5 mm when the width (c) is kept at 1.5 mm. When d is larger than 1.5 mm, the reflection coefficient does not change, although d changes. Therefore, we set the length (d) of the microfluidic channel as 2 mm.

#223429 - $15.00 USD Received 18 Sep 2014; revised 24 Nov 2014; accepted 10 Dec 2014; published 5 Jan 2015

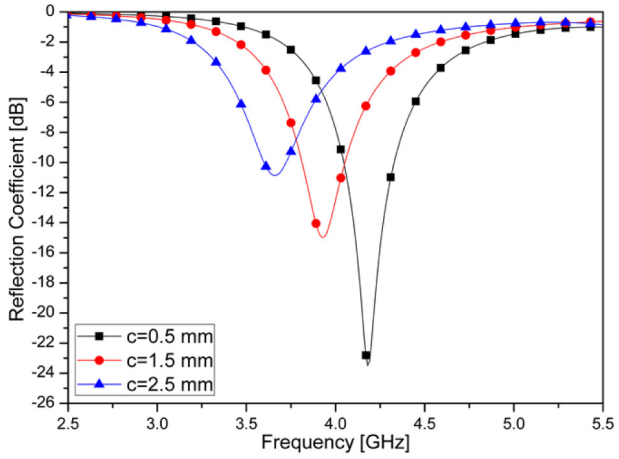

(a)

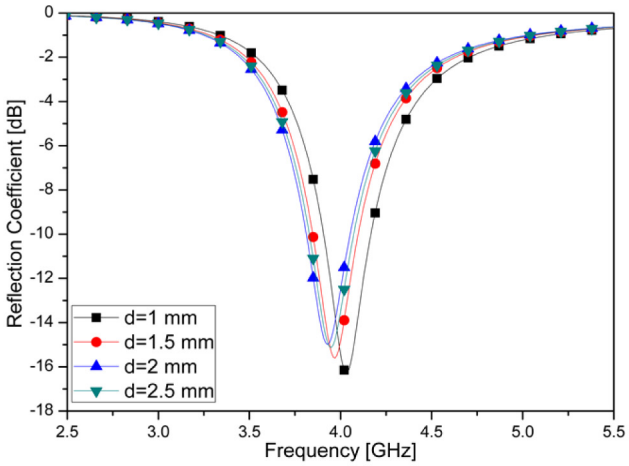

(b)

Fig. 4. Simulated reflection coefficients when the microfluidic channel is filled with distilled water. (a) The width (c) of the channel is 0.5 mm, 1.5 mm, and 2.5 mm at d = 2 mm. (b) The length (d) of the channel is 1 mm, 1.5 mm, 2 mm, and 2.5 mm at c = 1.5 mm.

To enable the injected fluids to flow, the capillary channels must be deployed to connect the rectangular cuboids, as shown in Fig. 5. Because the reflection coefficients do not change when the length (d) of the microfluidic channels is larger than 2 mm, the channels on the conductive patches can be arbitrarily designed. We showed three examples for channels on the conductive patch in Fig. 5 and simulated their reflection coefficients. As shown in Fig. 6, the channels on the conductive patch do not affect the reflection coefficients. Although the channels are asymmetric, we can expect polarization insensitivity. Therefore, we have freedom in designing the capillary channel. However, the capillary channel must be straight to prevent the formation of air bubbles and uneven filling. In order to minimize the number of inlets and outlets, we used a single path, which requires a single inlet and single outlet. When all capillary channels are straight, as illustrated in Fig. 5(b), the channels must intersect so that we cannot evenly fill fluids into the rectangular cuboids. Therefore, it is necessary to change the direction of the straight channel path. It is well-known that a channel

#223429 - $15.00 USD Received 18 Sep 2014; revised 24 Nov 2014; accepted 10 Dec 2014; published 5 Jan 2015

with a greater bend does not flow as smoothly. Therefore, Fig. 5(d) is the best option for smooth flowing because it is the least bent of the examples in Fig. 5.

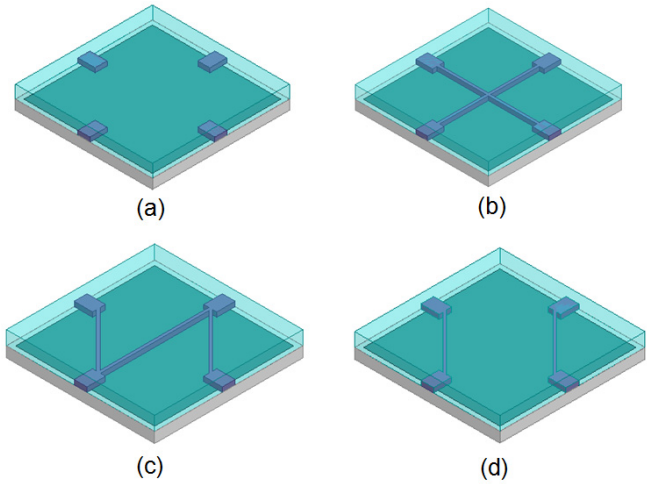

Fig. 5. Examples of capillary channel design for the unit cell: (a) without the capillary channel design, (b) cross-shaped channel design, (c) Z-type channel design, and (d) proposed channel design.

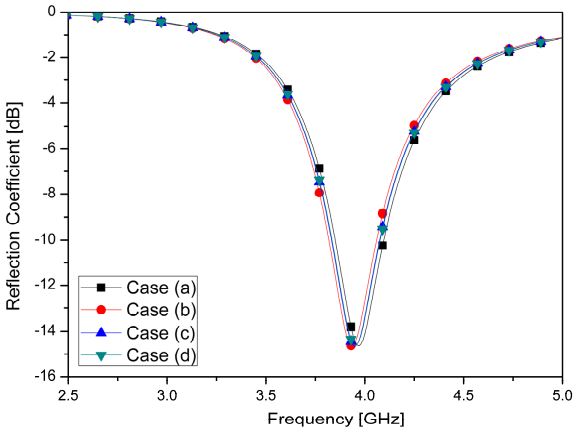

Fig. 6. Simulated reflection coefficients of four different unit cell geometries in Fig. 5.

3. Fabrication

Figure 7 illustrates the fabrication process, which comprises 5 steps: (1) etching the microfluidic channel, (2) printing the metallization layer, (3) printing the bonding layer, (4) bonding, and (5) finalization. The microfluidic channel is etched on 28-mm thick PMMA (McMaster-Carr, Atlanta, GA). We used an Epilog Legend EXT 120-W laser for laser-etching technology because it is simpler, cheaper, and faster than the photolithography process in a clean room. A 5-mm out-of-focus vector-mode laser beam is used, as calibrated in [22]. Two passes of a 24-W laser with 100% maximum speed are made to attain an ideal channel size. To connect the channel to the tubes, the inlet and outlet are cut using the same laser machine, but at a different setting. Three passes of an in-focus, vector-mode 40-W beam with 100% maximum speed are used to ensure that we cut through the 1.5-mm PMMA. The outline of the full-structure absorber is also cut using this setting.

#223429 - $15.00 USD Received 18 Sep 2014; revised 24 Nov 2014; accepted 10 Dec 2014; published 5 Jan 2015

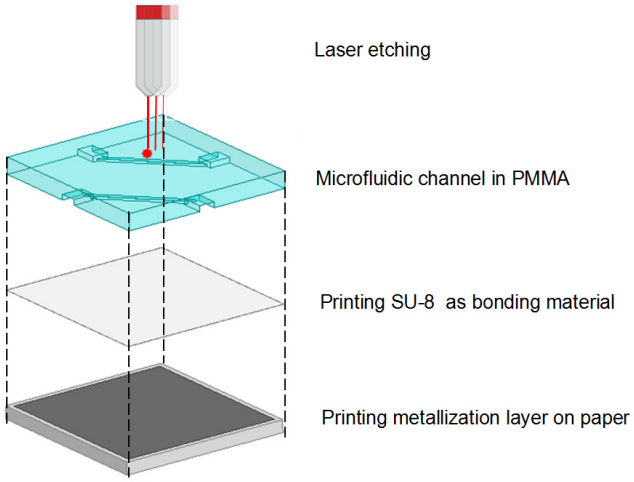

Fig. 7. Illustration of fabrication process for the proposed microfluidic inkjet-printed MM absorber.

The conductive square patches are inkjet-printed onto 220-µm-thick Kodak Premium Photo Paper (Office Depot, Atlanta, GA). ANP Silver-Jet 55LT-25C silver nanoparticle ink (Advanced Nano Products, Sejong, Korea) is used as the conductive ink for printing the metallization layer. The mixture of two SU-8 polymer solutions (MicroChem, Newton, MA) is used to bond the top microfluidic channel layer with the bottom conductive MM layer. The SU-8 bonding layer provides the additional function of isolating the fluid on the metallization layer. Gorilla Super Glue (Office Depot, Atlanta, GA) was used to strengthen the connection between the tubes and the inlets/outlets.

The inkjet-printing platform for the metallization layer and bonding layer is the Dimatix DMP-2831 materials deposition printer. We used a 20-µm drop space, a printer header temperature of 35°C, a printer platen temperature of 40°C, and a jetting frequency of 5 kHz for the ANP silver nanoparticle ink on paper. Three layers of the silver ink were printed to achieve a 0.1-Ω/square-sheet resistance. After printing the conductive patterns on the photo paper, it was put into a Thermo Scientific oven for 1 h at 120°C (because paper has a low burning point), and then for 5 min at 180°C to further enhance the conductivity.

In order to ensure adequate bonding between the paper and the PMMA, a layer of 28-µm adhesive polymers was printed on the photo paper using SU-8 solution, which was adjusted to enable printing with a Dimatix DMP-2831 material deposition printer. Achieving a suitable thickness of the bonding layer is crucial in the fabrication process. A thick bonding layer may lead to the microfluidic channel being blocked because the SU-8 solution will flow onto the microfluidic channel because of pressure that is applied to other areas during the bonding. On the other hand, a thin layer will result in poor bonding, which may cause leakage in some areas. Moreover, because SU-8 solution dries slowly in air, for a larger printing area that requires more time for printing, additional layers of SU-8 are needed. In this study, we decided to print four layers of SU-8 using the same setting as the silver ink, with one exception: the printer platen temperature was set to room temperature.

Several subsequent curing steps were required to ensure irreversible bonding. After we printed the bonding layer, the PMMA was flipped and squeezed onto the paper to remove any air between them. In order to soft bake the SU-8, the PMMA and paper were heated on a hot plate to 95°C for 4 min with a weight of 1 N/cm^2. The weight can protect the PMMA from warping and help ensure proper contact between the paper and SU-8 and between the PMMA and SU-8. Next, the fabricated MM absorber was exposed to 150 mJ/cm^2 of 254-nm

#223429 - $15.00 USD Received 18 Sep 2014; revised 24 Nov 2014; accepted 10 Dec 2014; published 5 Jan 2015

ultraviolet (UV) light with a CL-1000 UV Crosslinker. Finally, the absorber was heated to 95°C for 5 min, again with a weight of 1 N/cm^2 as a post-exposure bake.

Figure 8(a) shows a picture of the final fabricated microfluidic MM absorber prototype. In order to inject fluids, two tubes were secured to the inlet and outlet on the PMMA. As shown in Fig. 8(b), the fluid flows in one direction from the inlet through the microfluidic channel. The microfluidic channel and its cross section are magnified in Fig. 8(c) and 8(d), respectively.

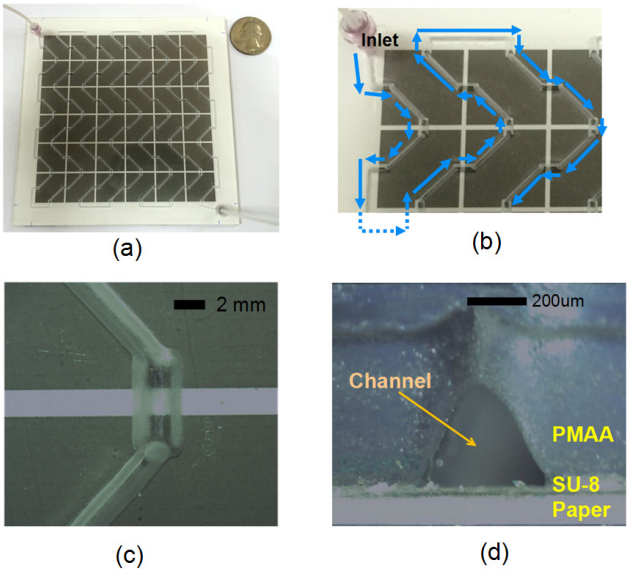

Fig. 8. Fabricated microfluidic MM absorber. (a) Top view of overall structure in 6 × 6 array configuration with inlet/outlet tubes. (b) Fluid flow in the channel of the unit cell (blur color). (c) Magnified view of the water-filled microfluidic channels on the gap between two square patches. (d) Cross section of the PMMA layer with the microfluidic channel.

4. Simulated and measured results

The absorptivity of the proposed absorber can be calculated by measuring the reflection coefficients using Eq. (3). The measurement setup is shown in Fig. 9. The transmission coefficients are assumed to be zero because the bottom plate is completely grounded. An Anritsu MS2038C vector network analyzer was used, and a horn antenna was placed horizontally on the wood tripod under normal incidence ($\theta = 0°$). To prevent interference due to undesired EM waves, we used the wedge-tapered absorber and time-gating method. Therefore, we measured only EM waves that were reflected from the proposed MM absorber sample.

To demonstrate the frequency-tuning capability of the proposed absorber, we injected distilled water into the empty microfluidic channel using a syringe. The simulated and measured absorptivity results at horizontal polarization ($\varphi = 0°$) are plotted in Fig. 10 for the empty microfluidic channel, which is filled with distilled water, ethanol, and tap water. For the empty channel, the proposed absorber shows a measured absorptivity of 98% at 4.42 GHz. Distilled water has already been characterized for full-wave simulations, and its dielectric constant and loss tangent are 66 and 0.16, respectively. After injecting the distilled water, the resonant frequency of the proposed absorber decreased to 3.97 GHz while maintaining its measured absorptivity at 94%. When the microfluidic channel is filled with ethanol and tap water, 93% and 90% absorptivity rates are still achieved at 4.31 GHz and 3.88 GHz, respectively. Ethanol has a dielectric constant of 23 and a loss tangent of 0.4. The

#223429 - $15.00 USD Received 18 Sep 2014; revised 24 Nov 2014; accepted 10 Dec 2014; published 5 Jan 2015

dielectric constant and loss tangent of tap water are 80 and 0.2, respectively. Therefore, we can conclude that the resonant frequency of the proposed absorber is dependent on fluid materials.

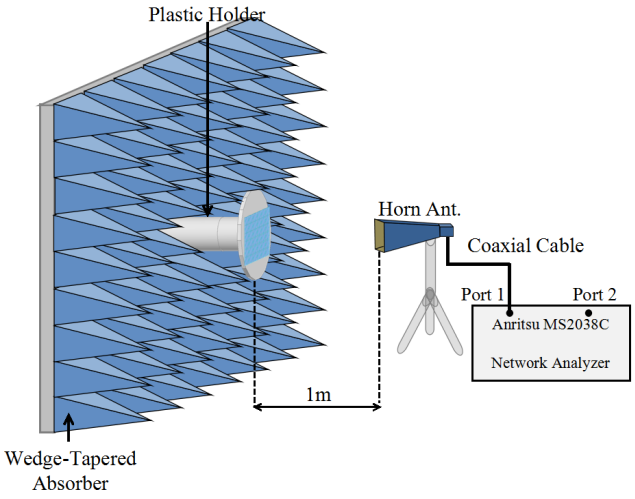

Fig. 9. Experimental setup to measure absorptivity.

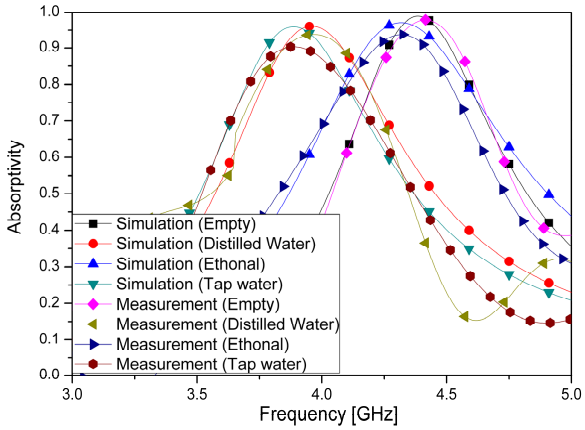

Fig. 10. Simulated and measured absorptivity when channel is empty and filled with distilled water, ethanol, and tap water.

Figure 11 shows the simulated and measured absorptivity with empty and water-filled channels at vertical (φ = 90°) and horizontal (φ = 0°) polarization. As we can expect, the absorptivity values are identical even though capillary channels on the patch are asymmetric. The proposed microfluidic MM absorber can be reused because the injected fluids can be removed though a syringe. We measured the absorptivity of the reused MM absorber after emptying the water-filled channel, and compared it with the absorptivity of the first MM absorber that we used. Figure 12 shows the measured absorptivity of three states: initial empty (first used), water-filled, and empty after filling (reused). The first-used and reused prototypes show almost identical results.

#223429 - $15.00 USD Received 18 Sep 2014; revised 24 Nov 2014; accepted 10 Dec 2014; published 5 Jan 2015

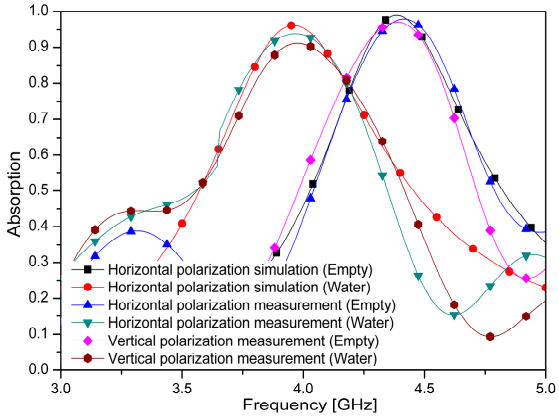

Fig. 11. Simulated and measured absorptivity with empty and distilled water-filled microfluidic channels for horizontal and vertical polarization incidence.

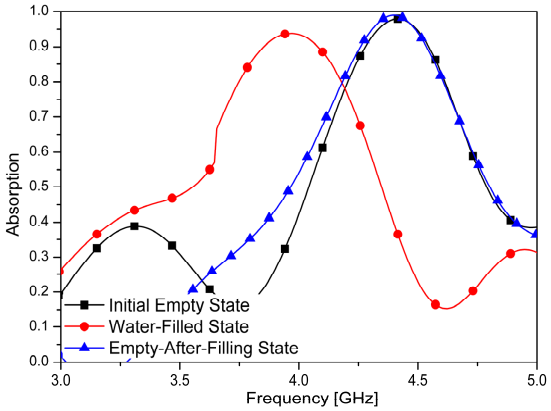

Fig. 12. Measured absorptivity of the proposed MM absorber at three states: initial empty (first used), water-filled, and empty after filling (reused).

5. Conclusion

We proposed a microfluidic tunable MM absorber whose frequency varies depending on the injected fluids. The absorber was fabricated with inkjet-printing technology for conductive patterns and bonding layers. The microfluidic channels were then etched using laser technology. Therefore, the fabrication process generated no chemical waste. The frequency-tuning capability of the proposed absorber was demonstrated in full-wave simulations and experiments by injecting distilled water into microfluidic channels. The frequencies varied from 4.42 GHz to 3.97 GHz after filling with water, while the absorptivity remained higher than 90% in both cases. In addition, both horizontal and vertical polarization incidence resulted in high absorptivity values. The proposed microfluidic MM absorber can be used as a frequency-tunable absorber as well as with wireless sensor platforms. Because the backside of the absorber is completely metallic, it can be attached to metallic objects. In addition, the fluidic-controllable resonance of the proposed absorber provides benefits for wireless chemical or biosensor applications. Inkjet-printing technology and organic paper substrates provide additional advantages for low-cost sensor applications.

Acknowledgments

This work was supported by Samsung Research Funding Center of Samsung Electronics under Project Number SRFC-IT1301-03.

#223429 - $15.00 USD Received 18 Sep 2014; revised 24 Nov 2014; accepted 10 Dec 2014; published 5 Jan 2015